JACS
JOURNAL OF THE AMERICAN CHEMICAL SOCIETY
Communication
pubs.acs.org/JACS

Visualizing Individual Carbon Nanotubes with Optical Microscopy

Michael A. Novak,[†] Sumedh Surwade,[†] Jason Prokop,[†] Kirill Bolotin,[‡] James Hone,[§] Louis Brus,[∥] Colin Nuckolls,*[,∥] and Haitao Liu*[,†]

[†]Department of Chemistry, University of Pittsburgh, Pittsburgh, Pennsylvania 15260, United States
[‡]Department of Physics, Vanderbilt University, Nashville, Tennessee 37212, United States
[§]Department of Mechanical Engineering and [∥]Department of Chemistry, Columbia University, New York, New York 10027, United States

Supporting Information

ABSTRACT: This paper reports a high-throughput, label-free technique to visualize individual carbon nanotubes (CNTs) on a silicon wafer using a conventional optical microscope. We show that individual CNTs can locally enhance the rate of vapor-phase HF etching of SiO_2 to produce a SiO_2 trench that is several to several tens of nanometers in depth. The trench is visible under an optical microscope due to a change in the optical interference in the SiO_2 layer, allowing the location of an individual CNT to be determined. With this technique, we demonstrate high-throughput Raman characterization and reactivity studies on individual CNTs.

Due to their superior electrical, mechanical, and optical properties, carbon nanotubes (CNTs) have found a wide range of applications in nanoelectronics, composite materials, energy conversion, and sensors.[1−9] The properties of CNTs can vary significantly depending on their structures. Unfortunately, there is no synthetic method that can produce pure CNTs of a single, defined chirality, but there have been significant advances in the postsynthesis separation of CNTs.[10−15] The limited availability of chirality-pure CNT samples has been a major obstacle in advancing their fundamental studies and applications.

One way to overcome the heterogeneity of the bulk sample is to study the properties and device performance of an individual CNT.[16−19] These studies all require locating individual CNTs under an optical microscope in order to carry out spectroscopic characterization or device fabrication. However, due to its small diameter, individual CNTs are invisible to conventional optical microscopy. One approach to address this challenge is to deposit optically visible markers (e.g., lithographically patterned gold film) on to the substrate and then use an atomic force microscope (AFM) or scanning electron microscope (SEM) to locate the CNTs relative the markers.[20] This process is both labor- and time-consuming and often contaminates the CNTs. Recently, two studies have shown that individual CNTs can be visualized under an optical microscope by decorating them with Ag or TiO_2 nanocrystals.[21,22] Although this approach is high throughput, the deposited material alters the intrinsic chemical and electrical properties (e.g., excited-state dynamics, charge doping) of the CNTs. In addition, these deposited materials are not compatible with certain chemical environments (e.g., strong oxidizing acid), and therefore the utility of this method is limited.

Herein we report a high-throughput, label-free technique for determining the precise location of an individual CNT using a conventional optical microscope. We show that CNTs locally enhance the vapor-phase HF etching of SiO_2, resulting in a nanoscale trench around itself (Figure 1A). Due to a change in the optical interference in the SiO_2 layer, the trench is visible under an optical microscope, allowing the position of the CNT to be determined (Figure 1B). Compared to previous methods to visualize CNT, the current method is high-throughput, low-cost, and label-free. These characteristics make it especially suitable for single-tube spectroscopy studies and device fabrications. Using this approach, we have carried out Raman characterization and reactivity study of individual CNTs.

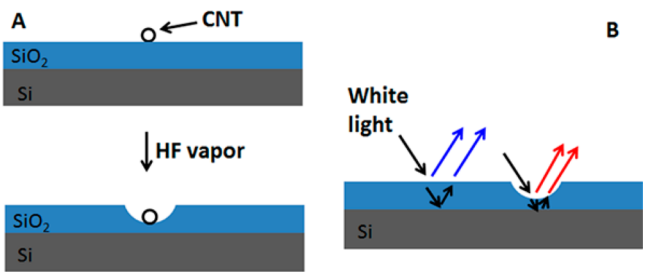

Figure 1. (A) CNT enhances the HF etching of SiO_2, producing a nanoscale trench around itself. (B) Change of optical interference (e.g., red vs blue) makes the trench visible under an optical microscope.

We grew ultralong CNTs using a previously reported chemical vapor deposition (CVD) method (see Supporting Information (SI) for details).[23] The substrate was a silicon wafer with 300 nm thick, thermally grown oxide on its surface. AFM images of the sample reveals that the CNTs were at least several hundred micrometers long, and their diameters typically ranged from 1−2 nm (Figures 2A and S1).

We found that the CNTs can locally enhance the vapor-phase HF etching of SiO_2 (Figure 1A). In a typical experiment, we exposed the CNTs sample to HF vapor inside a custom-built etching chamber (see the SI for details). We used AFM to

Received: April 16, 2014
Published: May 28, 2014

   dx.doi.org/10.1021/ja503821s | J. Am. Chem. Soc. 2014, 136, 8536−8539

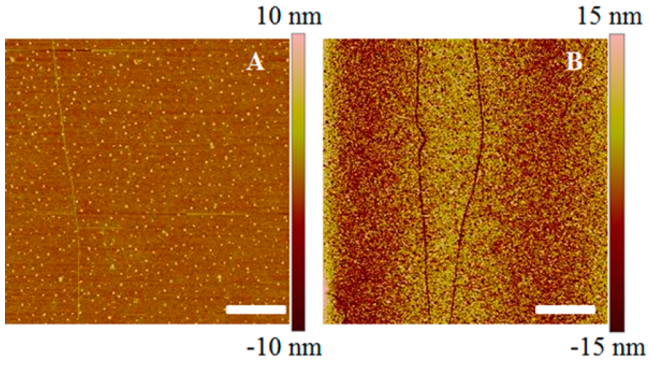

Figure 2. AFM images of (A) ultralong CNT and (B) trenches produced by CNT-enhanced HF etching of SiO_2. The scale bars in A and B represent 1 and 2 μm, respectively.

characterize the silicon wafer surface after the etching and the results are shown in Figure 2B. As can be seen, nanoscale trenches were present on the surface and no CNTs can be located. Detailed section analyses showed that the depth of the trenches ranged from several to several tens of nanometers. There was noticeable variation in the depth both within and between trenches (Figures S2 and S3); the reason for which is not yet understood. The shape of the trenches resembles that of the ultralong CNTs, suggesting that the CNTs are responsible for their formation. In one case, a section of CNT can be seen emerging from the trench after repeated AFM scan of the area (Figure S4). We believe that the AFM tip picked up the CNT and removed it out of the trench.

The trenches are visible under a conventional optical microscope, allowing the location of the associated CNT to be determined (Figure 3A). The visibility of the trench is due to a change in optical interference in the SiO_2 layer that strongly depends on its thickness.[24] For example, reducing the thickness of SiO_2 from 300 to 275 nm will result in a color change of the silicon wafer from blue/purple to red.[24] Figure 3B,C shows the AFM and optical micrographs collected on the same area of the sample. It can be seen that the shape of the trench in the optical image perfectly matched that of the trench in the AFM image. The appearance and contrast of the trench depend on the depth of the trench as well as the thickness of the SiO_2. Although we have not determined a quantitative relationship between the optical contrast and trench depth, trenches as shallow as 7 nm can be clearly visualized (Figures 3B and S3).

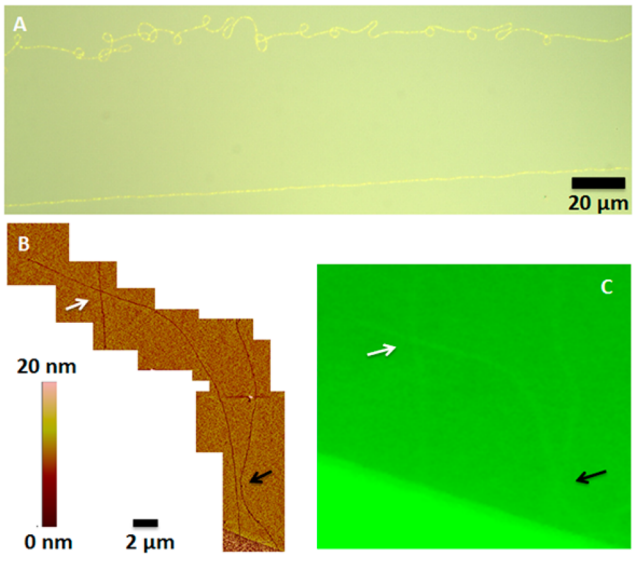

Figure 3. (A) Optical micrograph of two trenches produced by the CNT-enhanced HF etching of SiO_2. (B, C) AFM image mosaic and optical micrograph of the same area of a silicon wafer, respectively. The two sets of arrows indicate the same location.

The vapor-phase HF etching of SiO_2 is known to be sensitive to the surface concentration of water.[25] Water is a catalyst and also a reaction product of the reaction:

$$4HF + SiO_2 = SiF_4 + 2H_2O$$

The reaction is autocatalytic and the rate positively correlates with the local concentration of adsorbed water on the SiO_2 surface. We previously showed that DNA could enhance the vapor-phase HF etching of SiO_2 by promoting adsorption of water from the gas phase.[26] Preliminary results suggest that a similar mechanism is at play here.

We found that the etching rate of the SiO_2 in the absence of CNT decreased with increasing temperature. This observation is consistent with the hypothesis that high temperature reduces water adsorption on the surface. In addition, we have also studied the dependence of etching selectivity (i.e., the ratio of the etching rate in the presence of CNT to that in the absence of the CNT) as a function of reaction temperature. Figure S5 shows that the etching selectivity increases with increasing temperature until it reached a maximum at 90 °C. Further increase in the temperature resulted in a decrease in the selectivity instead. To understand this observation, we note that at low temperature, all surfaces, regardless of the presence of CNT, will be quickly saturated by the water produced by the HF etching reaction, resulting in nonselective etching. Similarly, at high temperature, water will completely desorb from all surfaces, resulting in a universal low etching rate and selectivity. The effect of CNTs is therefore most significant at intermediate temperature ranges. We note that the above analysis also underscores the importance to use vapor-phase HF etching instead of the more common solution phase etching process: in solution, the surface is saturated with water, and therefore the etching is not expected to produce deep trenches.

The fact that SiO_2 etching is faster in the presence of CNTs implies that CNTs enhance the adsorption of water. We note that previous studies also showed a similar effect from amorphous carbon produced by electron beam induced decomposition of hydrocarbon.[27] Noting that graphitic material was generally believed to be hydrophobic, the idea that CNTs enhance water adsorption may appear to be counterintuitive. However, recent studies have showed that the hydrophobicity of graphite and graphene are in fact due to airborne hydrocarbon contamination. A clean graphitic surface is in fact mildly hydrophilic.[28] In addition, it has also been suggested that when immersed in an aqueous solution, graphitic surface could selectively adsorb OH^- ions and by doing so alters the local pH near the surface.[29] We believe that both effects could contribute to an increase in the etching rate near the CNTs. Additional studies are needed to elucidate the detailed mechanism.

The ability to visualize CNTs with optical microscopy could greatly simplify many single-CNT studies. Compared to previous approaches to visualize individual CNTs, the present method has the distinct advantage of not having any foreign materials deposited onto the CNT and therefore will be

dx.doi.org/10.1021/ja503821s | J. Am. Chem. Soc. 2014, 136, 8536−8539

compatible with a wide range of physical and chemical processes. To demonstrate its potential usefulness, we have carried out micro-Raman characterization of individual CNTs to study their reactivity.

Due to the narrow absorption band of the CNTs,[19] only a small fraction of the trenches showed Raman peaks characteristic of CNTs when probed with a single laser. In all the Raman spectra we collected, we observed a very weak D peak. This is expected because HF is a weak, nonoxidizing acid and does not damage CNTs. In addition, almost all trenches showed the same Raman signatures throughout their length, indicating that the structure of the CNT was maintained during their growth. However, in one case, we observed a change in the Raman spectrum within a trench. Raman spectra of this CNT were taken at different locations, and a subset of the spectra is shown in Figure 4A. It can be seen that the spectra taken near the

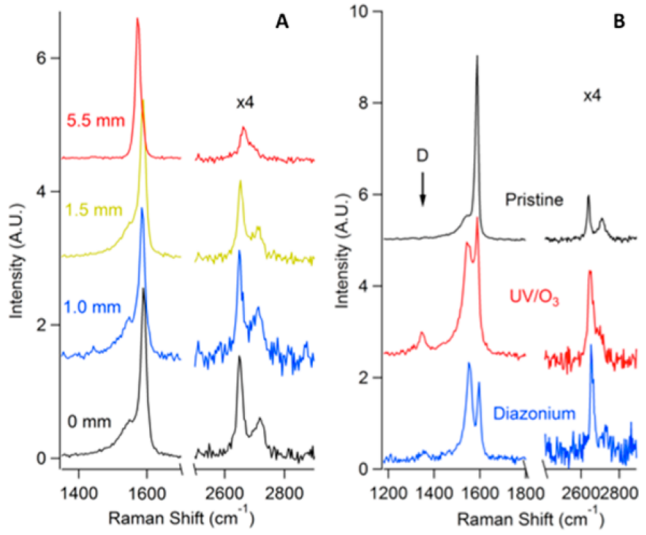

Figure 4. (A) Raman spectra (514 nm excitation) of an individual CNT collected at four different locations. The numbers represent the relative location of the sampling points along the CNT; larger value corresponds to further away from the catalyst. (B) Raman spectra of the same CNT before (black) and after UV/O_3 oxidation (red) and *p*-nitrobenzenediazonium (blue) functionalization. The arrow indicates location of the D peak. The spectra were scaled and shifted for clarity.

catalyst region showed two G' peaks and resolved G^- and G^+ peaks.[30] In contrast, only one G' peak was observed in the spectrum taken further away from the catalyst; the G peak region also showed only one peak. These data suggest a structural transition from a double-walled CNT to a single-walled CNT.[30] To verify this hypothesis, we have carried out UV/O_3 oxidation and *p*-nitrobenzenediazonium functionalization on two separate sections of this CNT where two G' peaks were present.[31,32] Shown in Figure 4b, after the reactions, we observed the appearance of the D peak at ~1350 cm^{-1} and the bleach of the G^+ peak at ~1587 cm^{-1}, both of which are consistent with chemical functionalization of the CNT. Notably, one of the G' peaks at ~2709 cm^{-1} disappeared, while no change was observed for the other G' peak at ~2639 cm^{-1}. The latter observation is consistent with the outer shell of a double-walled CNT undergoes chemical modification while the inner tube remained intact.[33,34]

Knowing the exact location of the CNT also allows one to track the progress of a reaction at the same location of an individual CNT. To demonstrate this possibility, we have carried out UV/O_3 oxidation of an individual semiconducting CNT that is 1.75 nm in diameter as determined by its Raman spectrum (see SI). Raman spectra were collected on the same location of the CNT (Figure S6) as a function of UV/O_3 exposure time, and a subset of the spectra is shown in Figure 5.

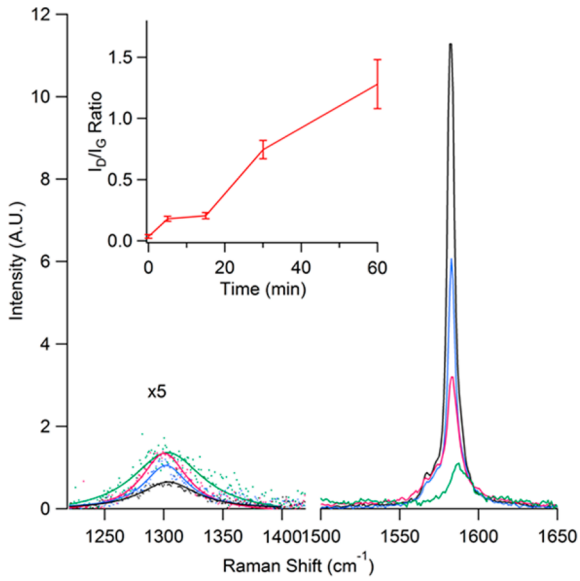

Figure 5. Raman spectrum of an individual CNT before (black) and after 5 min (blue), 15 min (red), and 30 min (green) of UV/O3 oxidation. All spectra were collected from the same location and under identical conditions using a 785 nm laser. The spectra were referenced and normalized using the Si overtone peak and shifted for clarity. For the D peak region, the dots are experimental data, and the lines are fits using a Lorentzian line shape. The inset shows the time evolution of the I_D/I_G ratio. The error bars represent the error associated with the peak fitting calculations.

Upon UV/O_3 oxidation, the D peak intensity increased while that of the G peak decreased. The decrease of G peak was previously attributed to a shift in the adsorption spectrum of CNT that leads to the loss of resonance in the Raman measurement.[35] The ratio of the intensity of D peak to that of the G peak (I_D/I_G) increased as a function of reaction time and this behavior resembles that observed in ensemble measurements (Figure 5 inset).

In conclusion, we have demonstrated a high-throughput approach to visualize individual CNTs under an optical microscope. Our approach takes advantage of the CNT-enhanced vapor-phase HF etching of SiO_2, which produces a nanoscale trench that is visible under an optical microscopy. Using the technique reported here, the synthesis and single-tube characterization of CNTs could be accomplished within a day. This approach is simple and compatible with a wide range of chemicals, making it especially suitable for studying reactivity of individual CNTs and fabrication of CNT and nanofluidic devices.[36]

■ ASSOCIATED CONTENT

Supporting Information

Experimental details and figures. This material is available free of charge via the Internet at http://pubs.acs.org.

dx.doi.org/10.1021/ja503821s | J. Am. Chem. Soc. 2014, 136, 8536−8539

AUTHOR INFORMATION

Corresponding Authors

hliu@pitt.edu
cn37@columbia.edu

Notes

The authors declare no competing financial interest.

ACKNOWLEDGMENTS

C.N. and L.E.B. were solely supported as part of the program "Center for Re-Defining Photovoltaic Efficiency Through Molecule Scale Control", an Energy Frontier Research Center funded by the U.S. Department of Energy, Office of Science, Office of Basic Energy Sciences under award no. DE-SC0001085. H.L. acknowledges AFOSR (FA9550-13-1-0083) and ONR (N000141310575) for partial support of this work.

REFERENCES

(1) Terrones, M. *Annu. Rev. Mater. Res.* **2003**, *33*, 419.
(2) De Volder, M. F. L.; Tawfick, S. H.; Baughman, R. H.; Hart, A. J. *Science* **2013**, *339*, 535.
(3) Wang, J. *Electroanal.* **2005**, *17*, 7.
(4) Endo, M.; Strano, M. S.; Ajayan, P. M. *Top. Appl. Phys.* **2008**, *111*, 13.
(5) Liu, Z.; Tabakman, S.; Welsher, K.; Dai, H. J. *Nano Res.* **2009**, *2*, 85.
(6) Barone, P. W.; Baik, S.; Heller, D. A.; Strano, M. S. *Nat. Mater.* **2005**, *4*, 86.
(7) Gabor, N. M.; Zhong, Z. H.; Bosnick, K.; Park, J.; McEuen, P. L. *Science* **2009**, *325*, 1367.
(8) Choi, W.; Hong, S.; Abrahamson, J. T.; Han, J. H.; Song, C.; Nair, N.; Baik, S.; Strano, M. S. *Nat. Mater.* **2010**, *9*, 423.
(9) Ajayan, P. M. *Chem. Rev.* **1999**, *99*, 1787.
(10) Zheng, M.; Jagota, A.; Strano, M. S.; Santos, A. P.; Barone, P.; Chou, S. G.; Diner, B. A.; Dresselhaus, M. S.; McLean, R. S.; Onoa, G. B.; Samsonidze, G. G.; Semke, E. D.; Usrey, M.; Walls, D. J. *Science* **2003**, *302*, 1545.
(11) Arnold, M. S.; Green, A. A.; Hulvat, J. F.; Stupp, S. I.; Hersam, M. C. *Nat. Nanotechnol.* **2006**, *1*, 60.
(12) Tu, X. M.; Manohar, S.; Jagota, A.; Zheng, M. *Nature* **2009**, *460*, 250.
(13) Hersam, M. C. *Nat. Nanotechnol.* **2008**, *3*, 387.
(14) Ghosh, S.; Bachilo, S. M.; Weisman, R. B. *Nat. Nanotechnol.* **2010**, *5*, 443.
(15) Liu, H. P.; Nishide, D.; Tanaka, T.; Kataura, H. *Nature Commun.* **2011**, *2*, 309.
(16) Duesberg, G. S.; Loa, I.; Burghard, M.; Syassen, K.; Roth, S. *Phys. Rev. Lett.* **2000**, *85*, 5436.
(17) Sfeir, M. Y.; Beetz, T.; Wang, F.; Huang, L. M.; Huang, X. M. H.; Huang, M. Y.; Hone, J.; O'Brien, S.; Misewich, J. A.; Heinz, T. F.; Wu, L. J.; Zhu, Y. M.; Brus, L. E. *Science* **2006**, *312*, 554.
(18) Hartschuh, A.; Pedrosa, H. N.; Novotny, L.; Krauss, T. D. *Science* **2003**, *301*, 1354.
(19) Dresselhaus, M. S.; Dresselhaus, G.; Jorio, A.; Souza, A. G.; Pimenta, M. A.; Saito, R. *Acc. Chem. Res.* **2002**, *35*, 1070.
(20) Liu, H. T.; He, J.; Tang, J. Y.; Liu, H.; Pang, P.; Cao, D.; Krstic, P.; Joseph, S.; Lindsay, S.; Nuckolls, C. *Science* **2010**, *327*, 64.
(21) Huang, S. M.; Qian, Y.; Chen, J. Y.; Cai, Q. R.; Wan, L.; Wang, S.; Hu, W. B. *J. Am. Chem. Soc.* **2008**, *130*, 11860.
(22) Zhang, R. F.; Zhang, Y. Y.; Zhang, Q.; Xie, H. H.; Wang, H. D.; Nie, J. Q.; Wen, Q.; Wei, F. *Nature Commun.* **2013**, *4*, 1727.
(23) Zheng, L. X.; O'Connell, M. J.; Doorn, S. K.; Liao, X. Z.; Zhao, Y. H.; Akhadov, E. A.; Hoffbauer, M. A.; Roop, B. J.; Jia, Q. X.; Dye, R. C.; Peterson, D. E.; Huang, S. M.; Liu, J.; Zhu, Y. T. *Nat. Mater.* **2004**, *3*, 673.
(24) Ghandhi, S. K. *VLSI fabrication principles: silicon and gallium arsenide*; Wiley: New York, 1983.
(25) Reinhardt, K. A.; Kern, W. *Handbook of silicon wafer cleaning technology*, 2nd ed.; William Andrew: Norwich, NY, 2008.
(26) Surwade, S. P.; Zhao, S. C.; Liu, H. T. *J. Am. Chem. Soc.* **2011**, *133*, 11868.
(27) Allgair, J.; Ryan, J. M.; Song, H. J.; Kozicki, M. N.; Whidden, T. K.; Ferry, D. K. *Nanotechnology* **1996**, *7*, 351.
(28) Li, Z. T.; Wang, Y. J.; Kozbial, A.; Shenoy, G.; Zhou, F.; McGinley, R.; Ireland, P.; Morganstein, B.; Kunkel, A.; Surwade, S. P.; Li, L.; Liu, H. T. *Nat. Mater.* **2013**, *12*, 925.
(29) Liu, H. T.; Steigerwald, M. L.; Nuckolls, C. *J. Am. Chem. Soc.* **2009**, *131*, 17034.
(30) Villalpando-Paez, F.; Son, H.; Nezich, D.; Hsieh, Y. P.; Kong, J.; Kim, Y. A.; Shimamoto, D.; Muramatsu, H.; Hayashi, T.; Endo, M.; Terrones, M.; Dresselhaus, M. S. *Nano Lett.* **2008**, *8*, 3879.
(31) Strano, M. S.; Dyke, C. A.; Usrey, M. L.; Barone, P. W.; Allen, M. J.; Shan, H. W.; Kittrell, C.; Hauge, R. H.; Tour, J. M.; Smalley, R. E. *Science* **2003**, *301*, 1519.
(32) Simmons, J. M.; Nichols, B. M.; Baker, S. E.; Marcus, M. S.; Castellini, O. M.; Lee, C. S.; Hamers, R. J.; Eriksson, M. A. *J. Phys. Chem. B* **2006**, *110*, 7113.
(33) Huang, J.; Ng, A. L.; Piao, Y. M.; Chen, C. F.; Green, A. A.; Sun, C. F.; Hersam, M. C.; Lee, C. S.; Wang, Y. H. *J. Am. Chem. Soc.* **2013**, *135*, 2306.
(34) Piao, Y. M.; Chen, C. F.; Green, A. A.; Kwon, H.; Hersam, M. C.; Lee, C. S.; Schatz, G. C.; Wang, Y. H. *J. Phys. Chem. Lett.* **2011**, *2*, 1577.
(35) Graupner, R. *J. Raman. Spectrosc.* **2007**, *38*, 673.
(36) Mijatovic, D.; Eijkel, J. C. T.; van den Berg, A. *Lab Chip* **2005**, *5*, 492.